Title

Propene Metathesis over Supported Tungsten Oxide Catalysts: A Study of Active Site Formation

Journal

ACS Catalysis, 6(11)

ISSN

2155-5435

Authors

Howell, John G
Li, Yi-Pei
Bell, Alexis T

Publication Date

2016-11-04

DOI

10.1021/acscatal.6b01842

Peer reviewed

ACS Catalysis

Research Article

pubs.acs.org/acscatalysis

Propene Metathesis over Supported Tungsten Oxide Catalysts: A Study of Active Site Formation

John G. Howell, Yi-Pei Li, and Alexis T. Bell*

Department of Chemical and Biomolecular Engineering, University of California, Berkeley, California 94720-1462, United States
Chemical Sciences Division, Lawrence Berkeley National Laboratory, Berkeley, California 94720, United States

Supporting Information

ABSTRACT: A detailed investigation was conducted on the factors influencing the properties of silica-supported tungsten oxide catalysts for propene metathesis. A principal goal of this work was to identify the processes involved in the formation of catalytically active sites. To probe the influence of dispersion, samples were prepared across a range of W loadings using two methods of catalyst preparation: incipient wetness impregnation of amorphous silica and ion exchange of mesoporous SBA-15. The samples were characterized by nitrogen adsorption, UV−vis, Raman, and X-ray absorption spectroscopy (XAS). Catalytic activity was observed to increase with W surface concentration up to the point where WO_3 nanoparticles formed. The catalytic performance of all samples was enhanced 2-fold by pretreatment in He, in comparison to pretreatment in air. In situ characterization of samples pretreated in He by Raman and XAS shows an increase in the relative concentration of isolated dioxo W(6+) species relative to mono-oxo W(6+) species, and in situ XAS data collected during propene metathesis indicated that a similar conversion occurs for air-pretreated samples in the presence of propene. For both air- and He-pretreated catalysts an activation period was observed, during which the activity increased and attained steady-state activity. This period was significantly longer for air-pretreated catalysts and was accompanied by the transient formation of acetone. While acetone was not observed during the much shorter transient of He-pretreated samples, in situ XAS provided evidence of reduction occurring in these samples upon contact with propene. It is also notable that, independent of the manner of catalyst preparation or pretreatment, the rate of propene metathesis is first order in propene and exhibits an activation energy of 200 kJ/mol. A model is proposed to explain why only a fraction of the isolated tungstate species is active for propene metathesis (∼5%) and why this fraction increases with increasing concentration of W dispersed on silica.

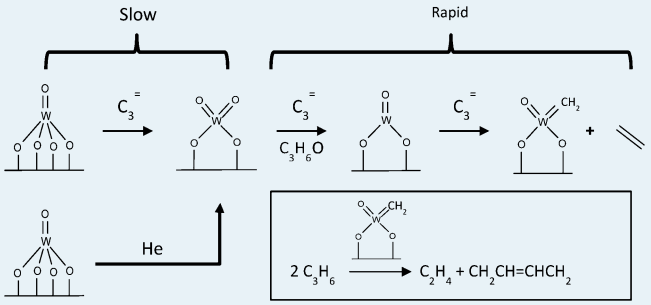

KEYWORDS: *propene, butene, metathesis, silica, tungstate species, catalyst activation*

1. INTRODUCTION

Olefin metathesis is a highly versatile process for interconverting olefinic hydrocarbons that has found numerous applications within the fuels, chemicals, and pharmaceutical industries.[1−4] Most investigations of olefin metathesis have involved homogeneous catalysts, particularly organometallic complexes of Re, Mo, W, and Ru. While such catalysts are highly effective for the stereoselective synthesis of pharmaceuticals and ring-opening polymerization, issues of cost, stability, and product separation have inhibited the use of homogeneous catalysts for large-scale production of commodity chemicals,[3] for which heterogeneous catalysts in the form of dispersed metal oxides have been found to be more suitable.[1] Examples include the Shell Higher Olefin Process (SHOP), the production of chemical feedstocks (e.g., neohexene), and the Philips Triolefin Process, which was originally designed for the production of ethene and butene from propene but is now run in the reverse direction (ABB Lummus) to meet the growing global demand for propene.[3]

Despite the long history of industrial use, the exact nature of the active sites involved in heterogeneously catalyzed olefin metathesis and the mechanism for this reaction are not known definitively.[1] Several authors have suggested that the mechanism for olefin metathesis over heterogeneous catalysts is analogous to that reported for homogeneous catalysts, which follows that proposed by Chauvin.[4,5] The reaction begins by binding of an alkene to a metal complex which contains a carbene ligand. Reaction of the coordinated alkene with the carbene produces a metallacyclic intermediate, which then decomposes to release the product alkene and generate a new carbene species. While it has been assumed that supported metal oxide catalysts follow a similar mechanism, direct observation of the active species and reaction intermediates has not been reported for such systems. There is consensus, though, that the reaction occurs preferentially, if not exclusively,

Received: July 1, 2016
Revised: September 23, 2016
Published: October 6, 2016

DOI: 10.1021/acscatal.6b01842
ACS Catal. 2016, 6, 7728−7738

over highly dispersed metal−oxo species bound to the catalyst support and that only a small fraction of such species is catalytically active (5−10%).[1,6] However, no direct evidence for carbene species or for the mechanism by which they are formed has been presented.[1,6,7]

Oxides of Re, Mo, and W have all been investigated for olefin metathesis.[1] While dispersed Re and Mo oxides are active at low to moderate temperatures, W oxide offers better stability, easier regeneration, and greater resistance to poisoning than supported Mo or Re oxides, and for these reasons dispersed W oxide is often preferred for large-scale industrial processes.[3,8,9] Extensive work on the characterization of supported tungsten oxides demonstrates the presence of species such as isolated mono-oxo ($(\equiv SiO)_4W{=}O$) or dioxo ($(\equiv SiO)_2W(=O)_2$) structures and dimeric and oligomeric tungsten surface species as well as bulk WO_3 nanoparticles.[10−12]

Previous investigations of propene metathesis over supported WO_x have shown that the rate of metathesis is approximately first order in the partial pressure of propene[13] and that pretreatment of the catalyst under an inert[7,14] or reducing gas[15] can enhance its activity relative to that observed after pretreatment in air. W loading has also been reported to influence catalyst performance, the rate of metathesis per atom of dispersed W increasing with increasing W loading up to the point where a substantial amount of WO_3 is formed.[9,14,16] The precursors to active species are proposed to be well-dispersed, isolated metal oxo species that in the presence of the reacting olefin convert into active metallocarbene species. Nevertheless, as noted in a recent review on metathesis on metal oxide catalysts, the exact nature of the influence of W loading and catalyst pretreatment on catalyst activity has not been established and there is no consensus on which tungsten oxide species are active for metathesis.[1]

The objective of this work is to elucidate the structure of active sites for propene metathesis over silica-supported tungsten oxide, to determine the distinguishing characteristics of precursors to active sites from those that remain spectators, and to gain insight into the formation of active centers. To this end, Raman, UV−vis, and X-ray absorption spectroscopy were used to characterize changes in the structure of WO_x species supported on silica as a function of W loading, catalyst pretreatment, and reaction in propene. The insights gained from these efforts enable us to propose a pathway by which dispersed tungsten oxo species are converted to catalytically active species and to provide suggestions for how W loading and pretreatment affect the concentration of active sites.

2. EXPERIMENTAL SECTION

2.1. Catalyst Preparation. Two approaches were used to produce silica-supported WO_x. The first was incipient wetness impregnation of amorphous silica gel with an aqueous solution of ammonium metatungstate (IWI-SiO_2). The second method involved the introduction of W via ion exchange with SBA-15, a high-surface-area mesoporous silica. The ion exchange procedure creates a more favorable binding environment between the metal ions in solution and the surface of the support, and the high-surface-area SBA-15 allows samples to be prepared over a wider range of W loadings. This allowed the effects of W loading and dispersion to be investigated in greater detail.

IWI-SiO_2 samples were prepared by incipient wetness impregnation of amorphous silica gel (Sigma-Aldrich) with an aqueous solution of ammonium metatungstate (Sigma-Aldrich). The concentration of AMT was varied to achieve the desired tungsten loading. The impregnated samples were then dried overnight at room temperature and calcined at 823 K for 5 h under a flow of dry air (100 cm^3/min).

Mesoporous SBA-15 was synthesized using a method adapted from Zhao et al.[17] Briefly, the triblock copolymer Pluronic P-123 (poly(ethylene glycol)-poly(propylene glycol)-poly(ethylene glycol)), was dissolved in a 0.20 M HCl solution, which was then stirred at room temperature to allow formation of surfactant micelles before adding the silica precursor, tetraethyl orthosilicate (TEOS). The stirred solution was heated to 313 K for 24 h, followed by heating under reflux for 24 h, which resulted in condensation of the silica precursor around the surfactant micelles. The slurry was then cooled, filtered, and dried overnight at room temperature. The composite silicate material was then suspended in ethanol to extract a portion of the surfactant in order to aid the subsequent calcination and again filtered and dried, after which the dry material was calcined in air at 823 K for complete removal of the surfactant.

The ion exchange (IE) method for tungsten incorporation was performed using a procedure adapted from ref 18. Briefly, the SBA-15 support was suspended in toluene and the suspension was heated to reflux before adding the functionalizing ligand, 3-aminopropyl trimethoxysilane (APTMS), using 3 mmol/g of support, and allowed to continue stirring at reflux for 24 h. The sample was then filtered, dried, and suspended in ethanol to remove loosely bound ligands. The collected sample was then suspended in a 0.3 M HCl solution to protonate the amine ligands, the suspension was again filtered and dried. The functionalized support was suspended in water, and the desired amount of AMT, dissolved in 5 mL of water, was added to the suspension for ion exchange. Finally, the collected sample was dried and calcined at 823 K to remove the amine ligands, leaving well-dispersed WO_x species on the surface of the silica support.

2.2. Catalyst Characterization. Tungsten loading was measured by Galbraith Laboratories in Knoxville, TN, using inductively coupled plasma optical emission spectroscopy (ICP-OES). Surface area, pore volume, and pore diameter were evaluated by nitrogen (Praxair, 99.999%) adsorption, using a Micromeritics Gemini VII BET instrument. Prior to all N_2 adsorption experiments, samples were degassed overnight at 393 K under vacuum to remove residual adsorbed water.

Diffuse reflectance UV−visible spectra were recorded using a Harrick Scientific diffuse reflectance attachment (DRP) and a Varian-Cary 6000i spectrophotometer. The spectra were acquired under ambient conditions. The edge energy (E_g) was determined by Tauc's law for indirect allowed transitions in amorphous and crystalline semiconductors.[19] A straight line was fit to the low-energy edge on a plot of $[F(R_1)h\nu]^{1/2}$ versus $h\nu$, where $F(R_1)$ is the Kubelka−Munk function and $h\nu$ is the incident photon energy. The edge energy is given by extrapolation of the linear region to the abscissa.

Raman spectra were acquired using a JobinYvon-Horiba spectrometer equipped with a confocal microscope and a 532 nm Nb/YAG laser. The laser line at 532 nm was removed from the backscattered light using an edge filter, and the filtered radiation was detected by a CCD detector (Andor) after passage dispersion by a grating (600 nm). Samples were prepared by lightly pressing the powder into a flat wafer. Spectra were acquired under ambient conditions or in situ

DOI: 10.1021/acscatal.6b01842
ACS Catal. 2016, 6, 7728−7738

using a Linkam CCR1000 catalytic reactor cell, using 10 mW of laser power at the sample.

X-ray adsorption (XAS) experiments were performed at the Advanced Photon Source at Argonne National Laboratory on beamlines BM-10-B and BM-4-D. The reported XANES data were acquired at the W L_1 edge, and the reported EXAFS data were acquired at the W L_3 edge. Sample pellets were pressed into a sample holder and placed in a horizontal quartz tube between two ionization chamber detectors. A W reference foil was placed after the second ionization chamber, allowing the collected sample spectra to be aligned to the foil. The spectra of W reference compounds were collected under ambient conditions. All data for catalyst samples were collected after pretreatment, which was performed in situ, using procedures identical with those used for collecting reaction data. Air pretreatments were performed at 823 K, and He pretreatments were performed at 873 K. After pretreatment, the samples were cooled to the reaction temperature of 693 K for spectral acquisition, in order to probe the nature of W sites under the reaction conditions. XAS data were analyzed using the Athena program of the IFEFFIT software package.

2.3. Measurement of Reaction Rates. Measurements of catalyst activity were performed using a 1/2 in. stainless steel reactor that was pinched in the middle to allow for the support of a fixed bed of catalyst. Quartz wool was placed inside the reactor, followed by 50 mg of catalyst diluted with 450 mg of amorphous silica. Additional quartz wool was placed on top of the catalyst. A K-type thermocouple was inserted directly into the fixed bed to monitor the temperature. Prior to each experiment, samples were pretreated in the reactor. Air pretreatment was performed using an abbreviated calcination procedure to represent the "as-synthesized" catalyst. For this, samples were heated to 823 K and held for 2 h under a 100 cm^3/min flow of dry air to remove residual moisture that may have been adsorbed during storage and reactor preparation. Helium pretreatments were performed by heating the samples at 873 K for 2 h under a 100 cm^3/min flow of He. After pretreatment, the reactor was cooled to the desired reaction temperature, and the sample was then contacted with propene (Praxair, 99.9%). Products were analyzed using an Agilent 7890A gas chromatograph (GC) equipped with a gas-sampling valve, a 30 m HP- Plot Q column, and a flame ionization detector.

3. RESULTS

3.1. Catalyst Characterization. Elemental composition and BET areas of IWI-SiO_2 and IE-SBA15 samples are presented in Tables S1 and S2 in the Supporting Information, respectively. The reported surface area (SA) is normalized for W loading and given in units of m^2/g of support, evaluated using the Brunauer–Emmett–Teller (BET) method for analysis of N_2 adsorption isotherms. The pore volume was evaluated by the Barrett–Joyner–Halenda (BJH) method, and the pore diameter was determined by the *t*-plot method.[20] The nominal surface concentration of W was calculated using the normalized BET surface area and reported as the number of tungsten atoms per square nanometer of support surface area. Over the range of loadings investigated, the structural parameters of catalyst samples remained largely unchanged, indicating that W exists as well -dispersed surface species that do not block the pores.

Raman spectra of IWI-SiO_2 samples and a spectrum of the pure silica support are presented in Figure 1. The spectrum for

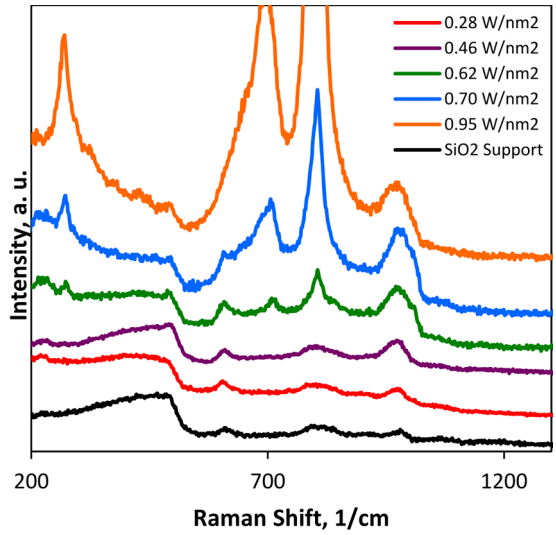

Figure 1. Raman spectra obtained under ambient conditions for IWI-SiO_2 samples of varying W loading. The spectra have been offset for clarity.

the SiO_2 support exhibits broad Raman features in the ranges of 400–500 and 800–900 cm^{-1} and a smaller feature at 610 cm^{-1}, corresponding to various breathing modes of the siloxane rings that make up the silica network, as well as an additional band at 975 cm^{-1} attributed to the Si–O stretching vibration of surface silanol groups.[10] At low W loadings (<0.5 W atoms/nm^2), the only noticeable change in the spectra is the growth of a broad band centered at 990 cm^{-1}, attributed to the combined features for symmetric and asymmetric stretching vibrations of terminally bound oxo ligands in dispersed WO_x species.[10−12] At intermediate loadings (0.6–0.7 W atoms/nm^2) the feature at 990 cm^{-1} continues to grow with W loading, suggesting a continued increase in the formation of WO_x species on the surface; however, new bands appear at 270, 720, and 805 cm^{-1} that increase in intensity with W loading. These features are attributable to bulk WO_3 nanoparticle formation and can be assigned to vibrational stretching frequencies (805 and 716 cm^{-1}) and the bending mode (270 cm^{-1}) of bridging W–O–W bonds.[10−12] It should be noted that the Raman scattering cross section for bulk WO_3 is much greater than that for surface species,[16] and therefore at the intermediate loadings the majority of W species are still present as well-dispersed monomeric or oligomeric WO_x species. As the W loading increases past 0.7 W atoms/nm^2, the bands characteristic of WO_3 continue to increase in intensity, while the band at 990 cm^{-1} does not increase further. At these higher loadings, the concentration of highly dispersed tungstate species cannot be increased further, and additional W incorporation contributes progressively to the growth of WO_3 nanoparticles.

The influence of W surface concentration on the band edge energies determined from UV–vis spectra of IWI-SiO_2 and IE-SBA15 are presented in Figure 2. Band edge energies, E_g, were also obtained for two reference compounds—Na_2WO_4, in which W is present as isolated tetrahedral centers (E_g = 4.7 eV), and bulk WO_3, in which W is present in octahedral centers (E_g = 2.3 eV). The edge energy, or band gap, for these materials is a measure of the ligand-to-metal ($O^{2-} \rightarrow W^{6+}$) charge transfer energy and is evaluated by a balance on the photon flux derived from the diffuse reflectance UV–visible spectra of the sample. It should be noted that the method for determining the band-

DOI: 10.1021/acscatal.6b01842
ACS Catal. 2016, 6, 7728–7738

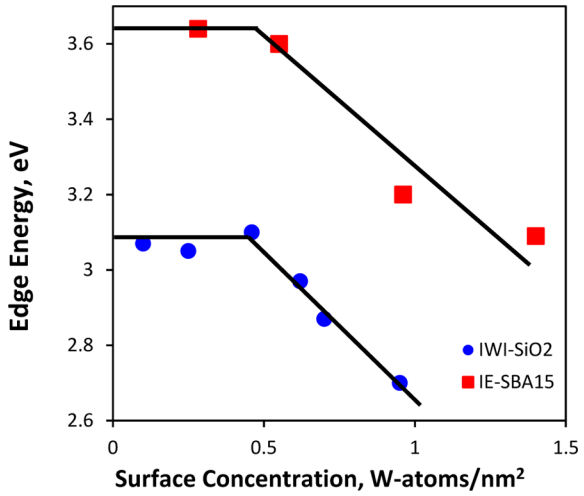

Figure 2. UV−vis edge energy values obtained for catalyst samples under ambient conditions as a function of tungsten loading.

edge energy depends on whether the transition is assumed to be direct or indirect, and both approaches have been used in the literature.[19] Because the materials used in the present study are amorphous, the crystal momentum is not conserved, and therefore an indirect transition has been used to calculate the edge energies. For such materials, the band gap is strongly influenced by the proximity and electronic interactions of neighboring W atoms, as a result of electron delocalization. Increasing the size of the WO_x clusters leads to a decrease in the band gap for the transition, and hence the band-edge energy is commonly used to evaluate the relative dispersion of metal sites in supported metal oxides.[10,11,19,21] The band-edge energy for IWI-SiO_2 samples (Figure 2) is approximately constant for W loadings below 0.5 W atoms/nm^2, suggesting that the nuclearity of the dispersed WO_x species is constant across this range of loadings. Above 0.5 W/nm^2 the band-edge energy decreases steadily, due to increasing W−W interactions associated with the formation of multimeric WO_x−surface species and ultimately bulk WO_3 nanoparticles. For all loadings, the band-edge energy for the IE-SBA15 samples is notably higher, in comparison to that for the IWI-SiO_2 samples, indicating that the relative dispersion of WO_x species is higher in these samples.

Characterization of as-prepared samples of WO_x dispersed on amorphous silica by IWI indicates that, for loadings below 0.6 W/nm^2, W is dispersed as isolated tungstate species and that, above this loading, an increasing fraction of the tungstate species form oligomers, containing W−O−W bonds. Raman spectroscopy also shows that, for W loadings above 0.5−0.6 W/nm^2, small particles of WO_3 are formed, which eventually become the dominant form of WO_x. Similar conclusions are drawn for the IE-SBA-15 samples, solely on the basis of the trends observed in the band-edge energies determined from UV−vis spectroscopy.

3.2. Activity for Propene Metathesis. Figure 3 shows plots of the turnover rate (TOR) for propene metathesis as a function of time on stream for air- and He-pretreated WO_x/SiO_2 prepared by incipient wetness impregnation of amorphous silica (IWI-SiO_2) (Figure 3a) and ion exchange of SBA-15 (IE-SBA15) (Figure 3b). Catalyst activity is reported as the moles of propene reacted per mole of W in the sample. For both methods of catalyst preparation, the TOR increases with time and then approaches a steady-state value. It is also observed that, irrespective of the manner of sample preparation, the air-activated catalyst reaches steady-state activity more slowly than the He-pretreated catalyst, and the steady-state activity is always lower for the air-pretreated catalyst. It should be noted that while the pretreatment in He was carried out at 873 K and that in air at 823 K, this difference in temperature is not responsible for the observed influence on activity. Thus, air pretreatment at 873 K did not increase the steady-state activity or affect the activation period relative to what was observed at 823 K. In agreement with previous reports,[7,14] the activity for propene metathesis increased with increasing temperature of the He pretreatment up to 873 K (see Figure S1 in the Supporting Information), above which no further enhancement in activity is observed.

The experiments reported in Figure 3 were carried out at 693 K in pure propene with a high weight hourly space velocity (WHSV) in order to eliminate external mass transfer limitations. For both methods of catalyst preparation the selectivity to the products of propene metathesis, ethene and butene, was >98%. The presence of 1-butene, resulting from the isomerization of the primary metathesis product, 2-butene, was observed but constituted only ∼5% of the $C_4^=$ fraction. Small quantities of C_5 and C_6 hydrocarbons were also observed

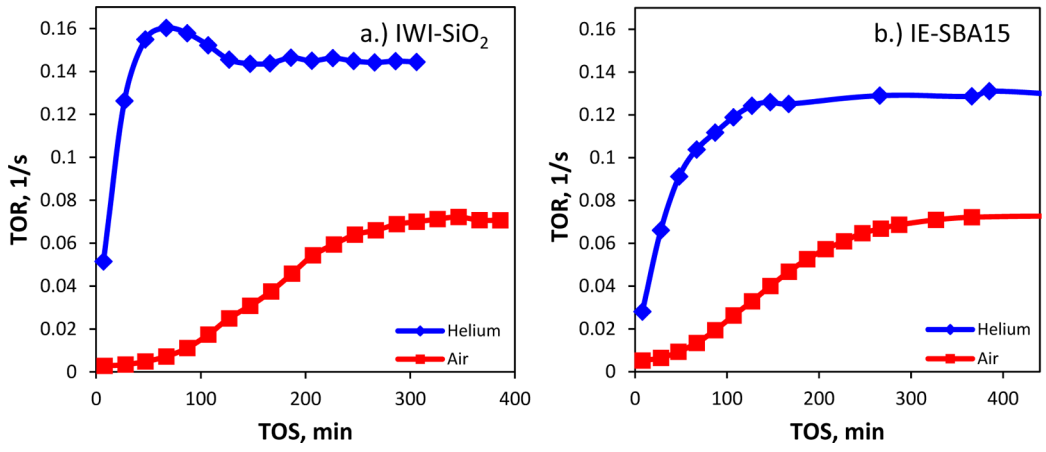

Figure 3. Time on stream activity (total W basis) for propene metathesis after air and He pretreatments: (a) for IWI-SiO_2 (0.6 W/nm^2); (b) for IE-SBA15 (1 W/nm^2). Conditions: $P_{tot} = P_{C3} = 1$ atm, $T = 693$ K, WHSV = 82 h^{-1}.

DOI: 10.1021/acscatal.6b01842
ACS Catal. 2016, 6, 7728−7738

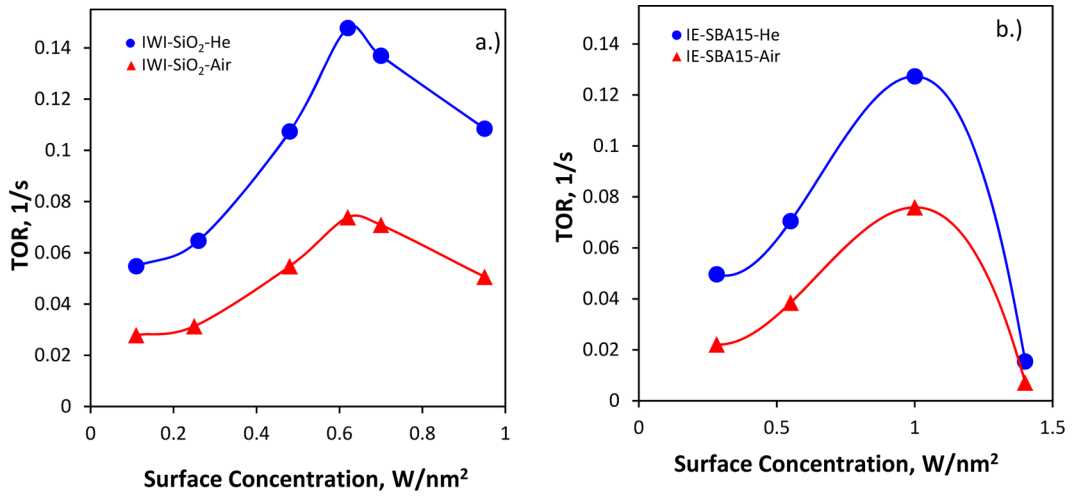

Figure 4. Steady-state activity for propene metathesis (moles of propene reacted per second per total moles of W) as a function of tungsten loading and pretreatment for (a) IWI-SiO_2 and (b) IE-SBA15 samples. Conditions: $P_{tot} = P_{C3} = 1$ atm, $T = 693$ K, WHSV = 82 h^{-1}.

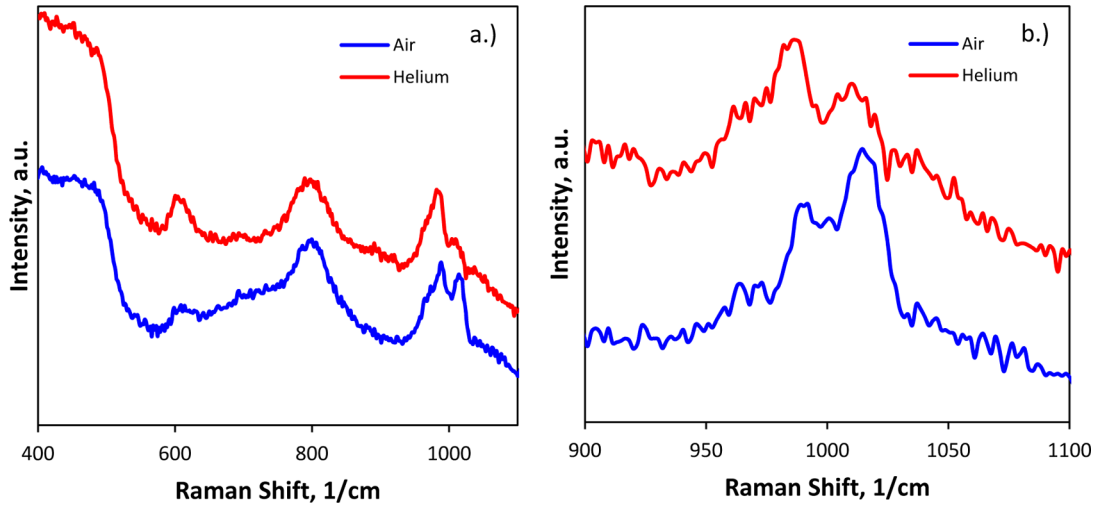

Figure 5. (a) In situ Raman spectra of IWI-SiO_2 (0.6 W/nm^2) collected at 693 K after air and He pretreatments. The spectra have been offset for clarity. (b) Region associated with the vibrational frequencies of W−oxo bond vibrations for pretreated samples after subtracting out the spectra of the pure silica support.

in the reactor effluent (<2%) and are attributed to a combination of secondary metathesis as well as acid-catalyzed reactions, such as isomerization, oligomerization, and cracking. These side reactions are attributable to the presence of Brønsted acid sites on the catalyst.

The steady-state activity for both pretreatment methods is shown in Figure 4 for a range of W loadings. For catalysts prepared by IWI, the TOR increases up to a maximum for 0.6 W/nm^2 and then decreases with further increases in W loading. The decrease in activity at loadings above 0.6 W/nm^2 is attributed to the formation of bulk WO_3 nanoparticles, as observed in the Raman spectra of these samples (Figure 1). This suggests that well-dispersed WO_x surface species are required to produce active centers for propene metathesis, in agreement with previous reports.[9,14,16] For all loadings, pretreating the catalyst in He enhances catalytic activity by approximately a factor of 2 relative to pretreatment in air. It is notable, though, that the apparent activation energy for propene metathesis, as determined by the Arrhenius relationship, is independent of both loading and pretreatment method: 200 ± 20 kJ/mol. This observation strongly suggests that the observed trends in activity are due to the number of active sites present, rather than any variation in the intrinsic activity of the catalytically active sites. Similar effects of catalyst pretreatment and W loading were observed for catalysts prepared by IE. The major difference in this case is that the maximum TOR occurs at about 1.0 W/nm^2. This difference is a direct consequence of the better dispersion of WO_x species on silica achieved by IE in comparison to IWI for a given W loading, ultimately increasing the dispersion limit (maximum W loading of well-dispersed surface species). However, the increase in dispersion does not appear to have a strong effect on the overall catalytic activity. It is notable that all of the catalysts prepared by IE also exhibited an apparent activation energy of 200 ± 20 kJ/mol for propene methathesis, identical with that observed for catalysts prepared by IWI. These results suggest that below a maximum W loading both methods of catalyst preparation produce virtually identical WO_x species. As noted earlier, both Raman and UV−visible spectra of as-prepared catalysts strongly suggest that the dispersed species are isolated tungstate species.

3.3. Changes in Catalyst Composition and Structure during Catalyst Break-In. Further investigations were

DOI: 10.1021/acscatal.6b01842
ACS Catal. 2016, 6, 7728−7738

undertaken with the aim of identifying the effects of pretreatment conditions on the structure of the isolated tungstate species present and further compositional and structural changes occurring during the rise in metathesis activity with time on stream (see Figure 3).

In situ Raman spectra were acquired in order to characterize the structure of the WO_x species present on the catalyst surface at the reaction temperature after pretreatment. As seen in Figure 5, following pretreatment in air at 823 K, two Raman features are observed near 1000 cm^{-1} attributable to W═O stretching vibrations. The feature at 1010−1020 cm^{-1} is assigned to the stretching vibration for W═O bonds in mono-oxo tungstate species, whereas the slightly broader feature at 950−995 cm^{-1} is assigned to the combined symmetric and asymmetric stretching vibrations for W═O bonds in dioxo tungstate species.[12,22] Comparison to the spectrum collected after He pretreatment reveals that the ratio of band intensities for dioxo versus mono-oxo species is higher following He pretreatment. The data suggest that pretreatment in He shifts the relative concentration of dioxo and mono-oxo species at the reaction temperature, leading to an increased concentration of dioxo sites on the catalyst surface.

The effects of sample pretreatment can also be detected in W L_1-edge XANES spectra. As seen in Figure 6, the position of the

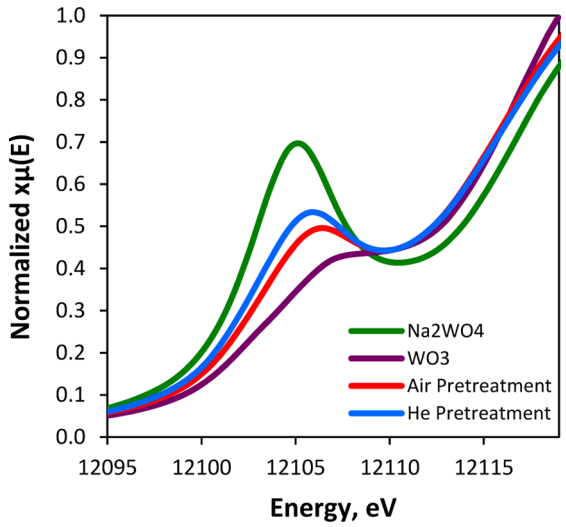

Figure 6. Normalized XANES spectra of W reference compounds and IWI-SiO_2 catalyst sample (0.6 W/nm^2) after different pretreatments.

edge indicates that, irrespective of treatment, W remains in the +6 oxidation state. The pre-edge feature near 12105 eV arises from the 2s to 5p transition.[23,24] This transition is Laporte forbidden for octahedral configurations, and only a slight shoulder is observed for W in the distorted-octahedral environment of WO_3. Extensive p−d orbital mixing in tetrahedral complexes leads to the large pre-edge feature observed for Na_2WO_4. The XANES spectrum of WO_x/SiO_2 (0.6 W/nm^2) prepared by IWI exhibits an intermediate-sized pre-edge feature, indicating the presence of p−d mixing from tetrahedral W sites. Previous studies of similar materials have shown that the size of the pre-edge feature can be used as a metric for evaluating the relative concentration of dioxo and mono-oxo surface species,[23,24] and this metric has been shown to be in agreement with DFT calculations and EXAFS data collected on the same samples.[23] As seen in Figure 6, spectra acquired following He pretreatment exhibit a pre-edge feature larger than for those pretreated in air, indicating a greater extent of p−d orbital mixing, providing further evidence that He pretreatment increases the relative concentration of tetrahedrally coordinated dioxo species.

The XANES and Raman data collected on catalyst samples after pretreatment, presented in Figures 5 and 6, indicate the presence of both dioxo and mono-oxo tungstate species and suggest that W(6+) mono-oxo species are converted to W(6+) dioxo species upon pretreatment in He. The higher proportion of dioxo species on the surface of He-treated samples, in comparison to the air-treated counterpart, provides a possible explanation for the increased steady-state activity exhibited by He-treated samples.

As noted in the discussion of Figure 3, the attainment of steady-state metathesis activity is preceded by a transient period of increasing activity. This period is very short (∼30 min) when the sample is pretreated in He and is much longer (∼240 min) when the sample is pretreated in air. Careful analysis of the products during the transient following air pretreatment enabled several interesting observations to be made. Figure 7

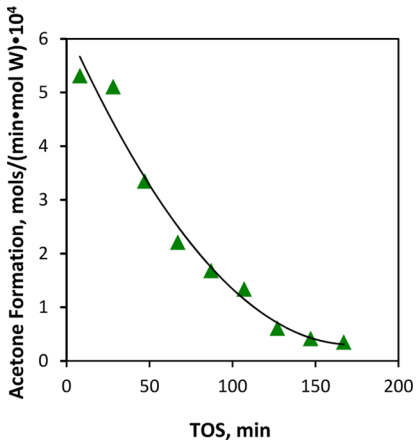

Figure 7. TOS activity for acetone formation after air pretreatment. Conditions: W loading 0.6 W/nm^2, P_{tot} = P_{C3} = 1 atm, T = 693 K, WHSV = 82 h^{-1}.

shows that in addition to the products of propene metathesis, ethene and butene, a small concentration of acetone is formed. The rate of acetone formation is highest at the onset of the reaction and decays with a time constant that is very similar to the time constant for the rise in metathesis activity. We attribute acetone formation to the partial reduction of a small amount of the W(6+) dioxo species to W(4+) mono-oxo species. Integration of acetone produced during the transient is equivalent to ∼5% of the tungsten in the sample containing 0.6 W/nm^2. It is also notable that the rate and amount of acetone formation are independent of the propene concentration in the gas phase.

Excess ethene formation was also observed, in addition to transient acetone production, during the catalyst activation period. The stoichiometry of propene metathesis should generate a 1:1 molar ratio of ethene and butene. However, upon initial exposure of the catalyst sample to propene, the ethene to butene molar ratio is notably larger than 1 and decreases with time on stream until it stabilizes at a value of 1.08 after about 150 min (Figure 8). Attempts were made to relate the quantity of acetone and excess ethene formed to the

DOI: 10.1021/acscatal.6b01842
ACS Catal. 2016, 6, 7728−7738

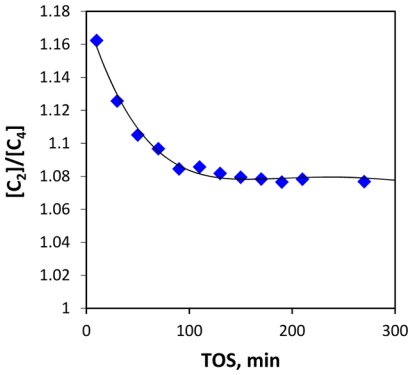

Figure 8. TOS activity for excess ethene formation after air pretreatment. Conditions: W loading 0.6 W/nm^2, P_{tot} = P_{C3} = 1 atm, T = 693 K, WHSV = 82 h^{-1}.

surface concentration of W loading; however, given the low concentrations of these transient products, no clear trend could be established. In contrast to the case of air-pretreated catalysts, neither acetone formation nor excess ethene could be observed during the short activation period for the catalyst pretreated in He.

In situ XANES data collected during the transient period upon first exposure to propene also reveal evidence for changes in the structure and composition of the supported WO_x species. Figure 9 shows how the W L_1 edge XANES spectrum changes with time for air- and He-pretreated WO_x/SiO_2 containing 0.6 W/nm^2 prepared by IE on SBA15. The principal change observed in both cases is a small decrease in the magnitude of the pre-edge feature. As can be seen in the inset to both parts pf Figure 9, the decline in pre-edge peak intensity is slower for the air-pretreated sample, in comparison to that of He pretreatment. It is also notable that the time constants for reaching steady state are similar in each case to those seen in Figure 3 for the transient approach to steady-state metathesis activity.

The decreasing pre-edge feature observed for both pretreatment cases is attributable to the reduction of W species or, alternatively, to changes in the geometry of grafted WO_x species. Both explanations have been shown to have a similar influence on the pre-edge feature in similar systems,[9,24,25] and thus it is impossible to define conclusively the structural changes occurring by analysis of the pre-edge feature alone. It is relevant to note that the main edge energy of the L_1 edge is largely unaffected by exposure of the catalyst sample to propene, which is consistent with the small extent of reduction expected on the basis of the observed formation of acetone.

W L_3 edge EXAFS data for air- and He-pretreated WO_x/SiO_2 are presented in Figure 10. The pretreated catalyst samples (Figure 10a) exhibit two large features in the first shell at 1.2 and 1.6 Å, attributed to W═O double bonds and W−O single bonds, respectively. The decreased size of the feature at 1.6 Å for the He-treated sample is consistent with the XANES and Raman analysis and provides additional evidence for a lower concentration of mono-oxo W sites after pretreatment in He. It is also noted that the absence of a large features near 4 Å, attributable to W−W scattering paths of multimeric W species,[25] supports the UV−vis results, suggesting that the majority of W exists as highly dispersed isolated tungstate species. Exposure of the air-pretreated sample to propene (Figure 10b) leads to a decrease in the intensities of the peaks for both W═O (1.2 Å) and W−O (1.6 Å). In contrast, Figure 10c shows that only the intensity of the peak for W═O decreases in intensity upon exposure of the He-treated sample to propene. This suggests that only W═O bonds of He-treated samples are affected by propene, while both the W═O and W−O bonds of the air-treated sample are affected. It is significant to point out that the decrease in intensity of the W−O peak upon exposure of the air-treated sample to propene closely resembles the decrease in intensity of that feature that occurs by pretreatment of the catalyst in He, suggesting that a similar transformation from mono-oxo to dioxo structure occurs when the air-pretreated sample is exposed to propene. We hypothesize that this may explain the slow activation of air-pretreated samples in comparison to the He-pretreated samples.

4. DISCUSSION

The preceding discussion shows that, independent of the type of silica used, the method of grafting isolated tungstate species onto the support (IWI or IE), and the method of pretreatment (air, He), the rate of propene metathesis is first order in propene partial pressure and has an apparent activation energy of 200 kJ/mol. These observations lead to the conclusion that the compositions and structures of the sites active for propene

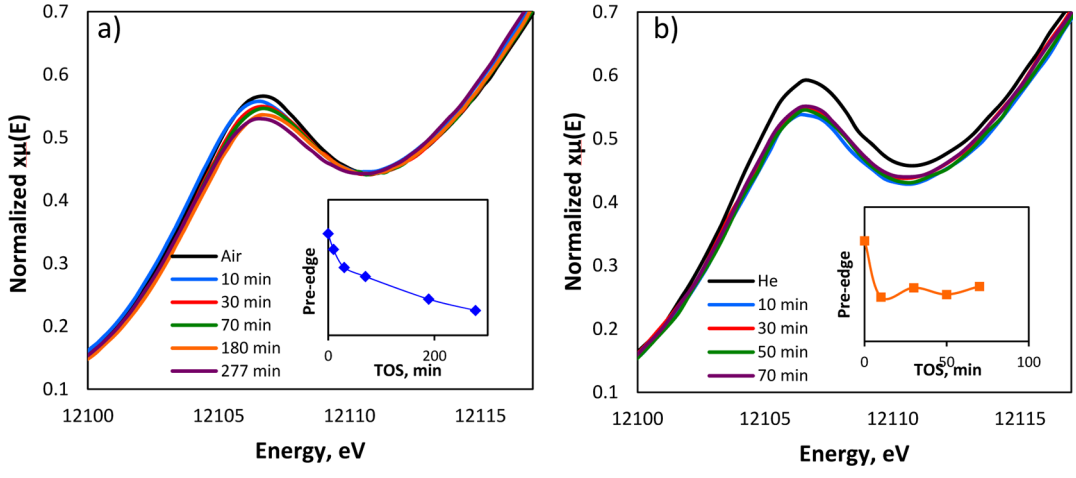

Figure 9. Normalized XANES spectra collected at the W L_1 edge for IE-SBA15 (0.6 W/nm^2) upon exposure to propene at 693 K for (a) air-pretreated and (b) He-pretreated samples. The variation in pre-edge height with TOS is shown in the insets.

DOI: 10.1021/acscatal.6b01842
ACS Catal. 2016, 6, 7728−7738

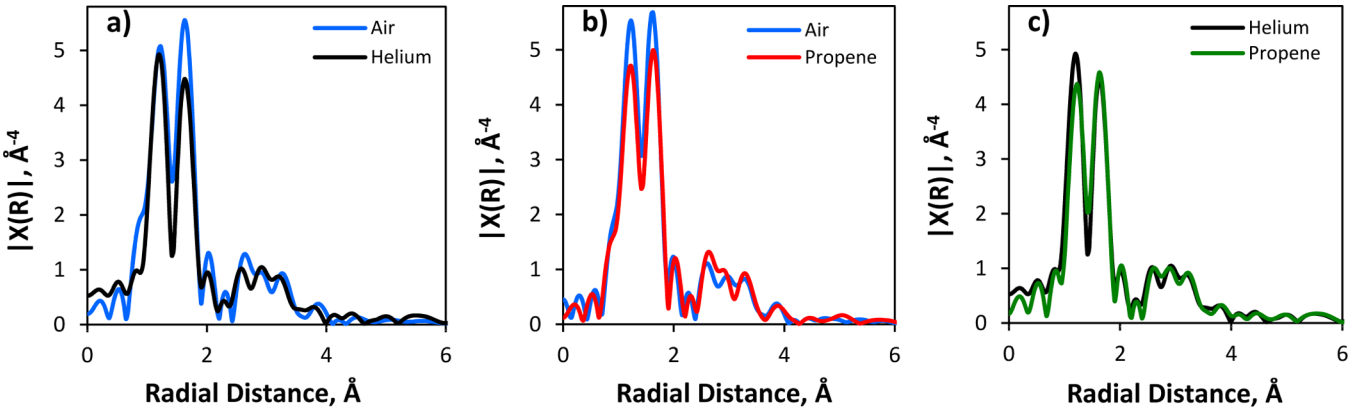

Figure 10. EXAFS spectra collected at the W L_3 edge for IE-SBA15 (0.6 W/nm^2) (a) after pretreatment and after reaching steady state in propene metathesis at 693 K for (b) air-treated and (c) He-treated samples.

Scheme 1. Illustration of the Structural and Compositional Changes Occurring during Air (a) and He (b) Pretreatments and during the Exposure of the Catalyst to Propene

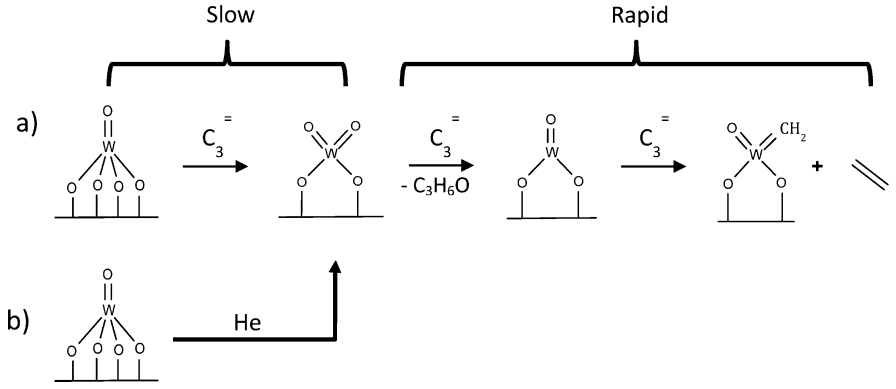

metathesis are identical in all cases. The questions then are as follows. (1) How are the active sites formed? (2) How does the manner of catalyst pretreatment affect the formation of active sites? (3) Why does the fraction of active sites change as the surface concentration of W increases?

Catalyst characterization after pretreatment and upon exposure to propene provides the information needed to address the first two questions posed above. The W edge energy determined from in situ XANES (Figure 6) indicates that, following either air or He pretreatment, all of the supported tungstate species are W(6+). In situ Raman spectra (Figure 5) provide evidence for both mono-oxo and dioxo tungstate species, irrespective of the mode of pretreatment; however, He pretreatment results in an increased proportion of dioxo species relative to that observed after air pretreatment. This conclusion is supported by in situ EXAFS data (Figure 10a), which show that the ratio of W═O to W−O bonds shifts in favor of the former following He pretreatment, in comparison to air pretreatment. Since He pretreatment leads to a more rapid approach to steady-state metathesis activity (see Figure 3), we propose that the conversion of mono-oxo tungstate species to dioxo tungstate species is an essential step along the path to forming active tungstate centers. This hypothesis is supported by the in situ EXAFS data obtained for the air-pretreated sample after exposure to propene (Figures 10b), which indicate a decrease in the W−O bond feature and resembles the change observed after He pretreatment.

A second step thought to be important for active site formation is the reduction of W(6+) dioxo species to form W(4+) mono-oxo species.[7,9] Supporting this idea is the observation of transient acetone formation upon exposure of the air-pretreated catalyst to propene seen in Figure 7. It is notable that the in situ EXAFS data presented in Figure 10b shows that, upon exposure of an air-pretreated sample of silica-supported WO_x to propene, the intensities of the peaks for both W═O and W−O features decrease in magnitude. We attribute these changes to the conversion of W(6+) mono-oxo species to W(6+) dioxo species, followed by reduction of the latter species to W(4+) species. The dynamics of the change in the pre-edge feature in the W L_1 edge XANES spectrum seen in Figure 9a are similar to those of the increase in the rate of propene metathesis for an air-pretreated catalyst (see Figure 3). While the transient formation of acetone could not be observed for a He-pretreated catalyst because the time scale for the approach to steady-state activity is much shorter than that of an air-pretreated catalyst, evidence for the reduction of W(6+) to W(4+) can be seen in the in situ W L_1 edge spectra shown in Figure 9b and in the in situ EXAFS data shown in Figure 10c. In the first of these figures, we note that the transient changes occur on the same time scale as the approach to steady-state metathesis activity, and in the second figure, only the peak characteristic of W═O bonds undergoes a reduction in intensity.

To further probe the influence of partial reduction in the formation of active tungstate centers, reactions were conducted on IWI-SiO_2 catalyst using a reducing pretreatment media (H_2 in He 10% by volume). As observed in Figure S2 in the Supporting Information, short exposure times (<10 min) to the

DOI: 10.1021/acscatal.6b01842
ACS Catal. 2016, 6, 7728−7738

reducing media provide an enhancement in steady-state activity, in comparison to air pretreatment, which is similar to that achieved by the He pretreatment. Additionally, the H_2/He-pretreated sample exhibits a higher initial rate for propene metathesis in comparison to that of the He pretreatment. These results provide further evidence that partial reduction of the W(6+) species of the as-synthesized catalyst is an important step in the formation of active tungstate centers.

The steps involved in the conversion of silica-supported tungstate species to active sites for the metathesis of propene are summarized in Scheme 1. Pretreatment in He bypasses the otherwise slow step in the active site formation process. We propose that the high-temperature treatment in He generates a larger concentration of these unstable dioxo sites, in comparison to that achieved by exposing an air-pretreated sample to propene, resulting in the higher steady-state activity exhibited by He-pretreated samples. The structural transformation from mono-oxo to dioxo species is a consequence of structural change occurring at elevated temperature, which is discussed in more detail below. The last step in the sequence in Scheme 1 is the reaction of propene with the W(4+) mono-oxo species to form a W(6+) oxo carbene species. While the latter species was not observed, Taoufik and co-workers[26] have prepared an oxo bisalkyl tungsten complex supported by two Si−O−W bonds on silica and demonstrated its activity for propene metathesis at 353 K. In this work, the supported complex is envisioned to produce the oxo carbene complex in situ; however, here again no experimental evidence was provided for the existence of the oxo carbene species.

Another question is why only a small fraction of the total W present on the catalyst surface is active for propene metathesis. The integral of the acetone transient indicates that, for a loading of 0.6 W/nm^2, only ∼5% of the total W atoms exposed are active. This value is similar to that reported previously for isolated molybdate species supported on silica and to that suggested previously for tungstate species supported on silica.[6,9] These observations suggest that the formation of oxo carbene species is a demanding process. To address this question, we carried out DFT calculations of both the enthalpy and Gibbs free energy required to convert $(\equiv SiO)_4W(=O)$ to $(\equiv SiO)_2W(=O)_2$ species and to then convert the latter species to the active species $(\equiv SiO)_2W(=O)(=CH_2)$ (see Scheme 1).

As shown in Figure 11, we assume that the W(6+) mono-oxo species ($(\equiv SiO)_4W(=O)$) are bound to a ring of four Si−O−Si units bonded together. Though the enthalpy change to convert this species in the presence of water vapor to ($(\equiv SiO)_2W(=O)_2$) plus two new Si−OH bonds is −41 kJ/mol (823 K), the corresponding Gibbs free energy change is 33 kJ/mol uphill due to the entropy loss of the consumption of a gas-phase water. This finding is consistent with the periodic DFT calculation recently reported by Handzlik and co-workers that the mono-oxo species ($(\equiv SiO)_4W(=O)$) is more favorable than the dioxo species ($(\equiv SiO)_2W(=O)_2$) at high temperature but the free energy difference between the two decreases as the temperature decreases.[22] The right-hand side of Figure 11 shows the enthalpy and Gibbs free energy changes required for the reaction of two propene molecules with $(\equiv SiO)_2W(=O)_2$ to form $(\equiv SiO)_2W(=O)(=CH_2)$, acetone, and ethene. In this case the enthalpy change is 169 kJ/mol and the Gibbs free energy change is 157 kJ/mol (693 K). While the standard-state Gibbs free energy change is high, under the reaction conditions, the steady-state concentration of acetone will be very low and consequently a small fraction of the ($\equiv SiO)_2W(=O)_2$ can undergo conversion to $(\equiv SiO)_2W(=O)(=CH_2)$ species.

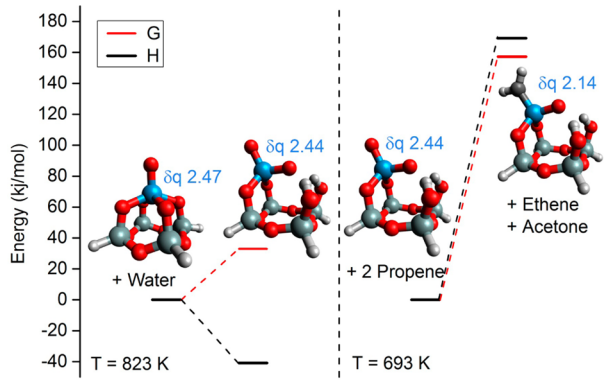

Figure 11. DFT calculated enthalpy and Gibbs free energy changes for (left) the conversion of $(\equiv Si-O)_4W=O$ to $(\equiv Si-O)_2W(=O)_2$ at 823 K and (right) the reaction of $(\equiv Si-O)_2W(=O)_2$ with two molecules of propene to form $(\equiv Si-O)_2W(=O)(=CH_2)$, acetone, and ethene at 693 K. Geometry optimizations and single-point energy calculations were carried out at the B97-D/Def2-SV(P) and ωB97X-V/Def2-TZVPD levels of theory, respectively. Thermodynamic corrections and entropies were calculated using the rigid rotor−harmonic oscillator model.

The question naturally arises as to why the conversion of $(\equiv SiO)_4W=O$ to $(\equiv SiO)_2W(=O)_2$ takes place via the reaction $(\equiv SiO)_4W=O + H_2O \rightarrow (\equiv SiO)_2W(=O)_2 + 2SiOH$, rather than via the reaction $(\equiv SiO)_4W=O \rightarrow (\equiv SiO)_2W(=O)_2 + Si-O-Si$, since at 823 K in He the catalyst should be free of water. To address this issue, we calculated the Gibbs free energy of reaction for the latter process is 100 kJ/mol at 823 K for the structure of $(\equiv SiO)_4W=O$ shown on the left-hand side of Figure 11. Since the Gibbs free energy change for the second reaction is so much greater than the first (100 vs 33 kJ/mol), we are led to conclude that small amounts of water are released, possibly by the condensation of surface silanol groups. It is also possible that species such as $(\equiv SiO)_2W(=O)(OH)_2$ react to form $(\equiv SiO)_2W(=O)_2$ species plus water, a process that might occur at elevated temperature if the initially grafted tungstate species do not fully coordinate with the surface during initial preparation of the catalyst. The estimated Gibbs free energy of reaction for this process is −45 kJ/mol, indicating that the reaction would occur spontaneously. It must be stressed, though, that further work is needed in order to determine more definitively how $(\equiv SiO)_4W=O$ species are converted to $(\equiv SiO)_2W(=O)_2$ species.

The third and final question is why the TOR reported in Figure 4 increases with the surface density of dispersed W. Since, as noted above, the dependence of the rate of propene metathesis on propene partial pressure and the activation energy are the same for all loadings below 0.6 W/nm^2, we conclude that all active sites are equivalent and, hence, the variation in the TOR seen in Figure 4 is a consequence of the fraction of W that is active, this fraction increasing with increasing W loading. The trend seen in this figure is similar to that which can be calculated from the data reported by Wachs and co-workers[9] for silica-supported tungstate species and those reported by Trunschke and co-workers[27] for silica-supported molybdate species. The authors of the latter study interpreted their observations by proposing that at low Mo coverage MoO_4 species are bonded to the silica surface in less strained configurations that are difficult to reduce but, as the

DOI: 10.1021/acscatal.6b01842
ACS Catal. 2016, 6, 7728−7738

Mo surface concentration increases, subsequent MoO_4 units bond in increasingly strained configurations, involving larger O−Mo−O bond angles that are more readily reduced. We envision that a similar process occurs for the W(6+) dioxo species formed by thermal conversion of W(6+) mono-oxo species. We therefore propose that the fraction of $(\equiv SiO)_2W(=O)_2$ species with O−W−O bond angles greater than ∼113° increases due to the increasing distance between Si−OH bonds involved in grafting WO_x species to the silica support. The increase in this bond angle results in a reduction in the energy needed to reduce $(\equiv SiO)_2W(=O)_2$ to $(\equiv SiO)_2W(=O)(=CH_2)$ species (see Figure 11), with the result that the surface concentration of the latter species will increase. While the absolute energies for the reduction of $(\equiv SiO)_2W(=O)_2$ to $(\equiv SiO)_2W(=O)(=CH_2)$ species is relatively large, this may be due to the simplicity of the model used to represent the surface and silica. Nevertheless, we believe that the influence of the O−W−O bond angle on the ease of forming active $(\equiv SiO)_2W(=O)(=CH_2)$ species provides a plausible explanation for the observed trend in the TOR reported in Figure 4.

5. CONCLUSIONS

Silica-supported tungsten oxides prepared by incipient wetness impregnation and ion exchange were investigated in detail to establish the effects of W loading and catalyst pretreatment on the structure of the dispersed species and their activity for propene metathesis. Characterization of as-prepared samples revealed that isolated tungstate species prevail below a loading of 0.6 W/nm^2 for materials prepared by incipient wetness on amorphous silica and for loadings below 1.0 W/nm^2 for materials prepared by ion exchange on SBA-15. For both methods of catalyst preparation, the steady-state rate of propene metathesis per W atom (TOR) increases with W surface coverage up to a maximum that occurs at the surface coverage at which nanoparticles of WO_3 are detected by Raman spectroscopy. It is also observed that pretreatment in air at 823 K and in He at 873 K affected the steady-state activity, with He pretreatment resulting in a 2-fold higher TOR. However, independent of W dispersion or catalyst pretreatment the rate of propene metathesis is first order in propene and has an activation energy of 200 kJ/mol.

In situ Raman, W L_1 edge XANES, and W L_3 edge EXAFS characterization of pretreated catalysts containing 0.6 W/nm^2 indicate the presence of isolated mono-oxo and dioxo W(6+) species ($(\equiv SiO)_4W(=O)$ and $(\equiv SiO)_2W(=O)_2$), the proportion of dioxo to mono-oxo species being higher following He pretreatment. Upon exposure to propene, both air- and He-pretreated samples exhibit a transient approach to steady-state activity. This period is significantly longer for the air-pretreated sample and is accompanied by the transient production of acetone. Integration of the acetone transient suggests that about 5% of the dispersed W undergoes reduction. Because of the much shorter duration, similar data could not be obtained for the He-pretreated sample. W L_1 edge XANES characterization of both air- and He-pretreated samples shows a transient in the pre-edge feature characteristic, the dynamics of which are nearly identical with those of the transient in the rise in metathesis activity. The transients in the L_1 edge XANES spectra are attributed to the reduction of W(6+) to W(4+) oxo species, a conclusion supported by in situ W L_3 edge EXAFS data. On the basis of these findings, we propose the sequence of elementary processes shown in Scheme 1, via which $(\equiv SiO)_4W(=O)$ structures are converted to $(\equiv SiO)_2W(=O)_2$ structure upon pretreatment and the latter structure is reduced to $(\equiv SiO)_2W(=O)$ structures and acetone upon exposure to propene under the reaction conditions. We further propose that $(\equiv SiO)_2W(=O)$ structures react with additional propene to form $(\equiv SiO)_2W(=O)(=CH_2)$ species, the active centers involved in propene metathesis, and ethene. DFT estimates of the energy required for the conversion of $(\equiv SiO)_4W(=O)$ to $(\equiv SiO)_2W(=O)_2$ species and the reduction of the latter species to $(\equiv SiO)_2W(=O)$ species suggest that, while the first of these steps is mildly endothermic and highly dependent on the magnitude of the O−W−O bond in the $(\equiv SiO)_2W(=O)_2$ species, the reduction of $(\equiv SiO)_2W(=O)_2$ species by propene to produce $(\equiv SiO)_2W(=O)$ species and acetone is significantly more demanding energetically and, hence, may only occur if the reacting tungstate species are in a high-energy state due to structural deformation. Finally, our calculations suggest that the reaction of $(\equiv SiO)_2W(=O)$ species with propene to form $(\equiv SiO)_2W(=O)(=CH_2)$ species and ethene is nearly thermoneutral. We believe that the results of the present investigation and their discussion provide significant new insights into the processes involved in the conversion of as-prepared silica-supported tungstate species into tungstate species that are active for propene metathesis and help to explain why only a small fraction of the dispersed tungstate species becomes catalytically active and why this fraction increases with tungsten loading.

■ ASSOCIATED CONTENT

Supporting Information

The Supporting Information is available free of charge on the ACS Publications website at DOI: 10.1021/acscatal.6b01842.

Nitrogen adsorption data of catalyst samples, effect of He pretreatment temperature on catalyst activity, and effect of H_2 pretreatment on catalyst activity (PDF)

■ AUTHOR INFORMATION

Corresponding Author

*E-mail for A.T.B.: bell@cchem.berkeley.edu.

Notes

The authors declare no competing financial interest.

■ REFERENCES

(1) Lwin, S.; Wachs, I. *ACS Catal.* **2014**, *4*, 2505−2520.
(2) Banks, R. *ACS Symp. Ser.* **1983**, *222*, 403−414.
(3) Mol, J. *J. Mol. Catal. A: Chem.* **2004**, *213*, 39−45.
(4) Hoveyda, A.; Zhugralin, A. *Nature* **2007**, *450*, 243−251.
(5) Hérisson, J.; Chauvin, Y. *Makromol. Chem.* **1971**, *141*, 161−176.
(6) Amakawa, K.; Wrabetz, S.; Kröhnert, J.; Tzolova-Müller, G.; Schlögl, R.; Trunschke, A. *J. Am. Chem. Soc.* **2012**, *134*, 11462−11473.
(7) Basrur, A.; Patwardhan, S.; Vyas, S. *J. Catal.* **1991**, *127*, 86−95.
(8) Heckelsberg, L.; Banks, R.; Bailey, G. *Ind. Eng. Chem. Prod. Res. Dev.* **1968**, *7*, 29−31.
(9) Lwin, S.; Li, Y.; Frenkel, A.; Wachs, I. *ACS Catal.* **2016**, *6*, 3061−3071.
(10) Lee, E.; Wachs, I. *J. Phys. Chem. C* **2007**, *111*, 14410−14425.
(11) Ross-Medgaarden, E.; Wachs, I. *J. Phys. Chem. C* **2007**, *111*, 15089−15099.
(12) Lee, E.; Wachs, I. *J. Phys. Chem. C* **2008**, *112*, 6487−6498.
(13) Luckner, R.; McConchie, G.; Wills, G. *J. Catal.* **1973**, *28*, 63−68.
(14) Andreini, A.; Mol, J. *J. Colloid Interface Sci.* **1981**, *84*, 57−65.
(15) Westhoff, R.; Moulijn, J. *J. Catal.* **1977**, *46*, 414−416.

DOI: 10.1021/acscatal.6b01842
ACS Catal. 2016, 6, 7728−7738

(16) Thomas, R.; Moulijn, J.; De Beer, V.; Medema, J. *J. Mol. Catal.* **1980**, *8*, 161−174.
(17) Zhao, D.; Huo, Q.; Feng, J.; Chmelka, B. F.; Stucky, G. D. *J. Am. Chem. Soc.* **1998**, *120*, 6024−6036.
(18) Shylesh, S.; Singh, A. *J. Catal.* **2006**, *244*, 52−64.
(19) Barton, D.; Shtein, M.; Wilson, R.; Soled, S.; Iglesia, E. *J. Phys. Chem. B* **1999**, *103*, 630−640.
(20) Somorjai, G.; Li, K. *Introduction to Surface Chemistry and Catalysis*; Wiley: Hoboken, NJ, 2010.
(21) Weber, S. *J. Catal.* **1995**, *151*, 470−474.
(22) Guesmi, H.; Grybos, R.; Handzlik, J.; Tielens, F. *RSC Adv.* **2016**, *6*, 39424−39432.
(23) Yamazoe, S.; Hitomi, Y.; Shishido, T.; Tanaka, T. *J. Phys. Chem. C* **2008**, *112*, 6869−6879.
(24) Yamamoto, T.; Orita, A.; Tanaka, T. *X-Ray Spectrom.* **2008**, *37*, 226−231.
(25) Hilbrig, F.; Gobel, H.; Knozinger, H.; Lengeler, B. *J. Phys. Chem.* **1991**, *95*, 6973−6978.
(26) Bouhoute, Y.; Grekov, D.; Szeto, K.; Merle, N.; De Mallmann, A.; Lefebvre, F.; Raffa, G.; Del Rosal, I.; Maron, L.; Gauvin, R.; Delevoye, L.; Taoufik, M. *ACS Catal.* **2016**, *6*, 1−18.
(27) Amakawa, K.; Sun, L.; Guo, C.; Hävecker, M.; Kube, P.; Wachs, I.; Lwin, S.; Frenkel, A.; Patolla, A.; Hermann, K.; Schlögl, R.; Trunschke, A. *Angew. Chem., Int. Ed.* **2013**, *52*, 13553−13557.

DOI: 10.1021/acscatal.6b01842
ACS Catal. 2016, 6, 7728−7738